Available online at www.sciencedirect.com
SCIENCE DIRECT
Journal of Catalysis 226 (2004) 372–381
JOURNAL OF CATALYSIS
www.elsevier.com/locate/jcat

The effect of Pt–Rh synergism on the thermal stability of rhodium oxide on pure alumina and Ce–ZrO_2-modified alumina-supported catalysts

R. Polvinen [a], M. Vippola [b], M. Valden [a,*], T. Lepistö [b], A. Suopanki [c], M. Härkönen [c]

[a] *Surface Science Laboratory, Tampere University of Technology, PO Box 692, FIN-33101, Tampere, Finland*
[b] *Institute of Materials Science, Tampere University of Technology, PO Box 589, FIN-33101 Tampere, Finland*
[c] *ECOCAT Oy, Catalyst Research, PO Box 171, FIN-90101, Oulu, Finland*

Received 22 March 2004; revised 6 May 2004; accepted 31 May 2004

Available online 8 July 2004

Abstract

Pt, Rh, and bimetallic Pt–Rh catalysts with pure alumina and Ce–ZrO_2-modified alumina washcoats are studied by XPS and TEM. The synergistic effect of platinum and rhodium is shown to be capable of stabilizing rhodium against the formation of a reduction-resistive oxide phase on alumina-supported catalysts in high-temperature air aging. Rhodium is found to exist in two different states: reduction-resistive rhodium oxide in strong interaction with alumina support and reducible rhodium oxide on the surface of Pt–Rh bimetallic particles. The growth of the noble metal particle size in the aging treatment is observed to be more pronounced on the Ce–ZrO_2-containing catalysts than on pure alumina-supported catalysts. Moreover, further increase of the particle size is detected on the Ce–ZrO_2-containing catalysts after H_2 reduction at 300 °C. This may be related to the ability of Ce–ZrO_2 to release oxygen in reducing atmosphere.

Keywords: Rhodium; Platinum; Bimetallic; X-ray photoelectron spectroscopy; Transmission electron microscopy; Supported catalyst

1. Introduction

Platinum and rhodium have been widely used as active components in automotive three-way catalysts (TWCs). The main role of platinum is to operate as an oxidation catalyst for carbon monoxide and unburned hydrocarbons, while rhodium is highly active in the reduction of nitric oxides to nitrogen. Bimetallic catalysts often exhibit properties better than shown by either of the single metal catalysts, for example, improved activity, selectivity, or thermal stability. This kind of behavior is called synergistic behavior or synergistic effect of the two metals. The presence of the synergistic activity effects of platinum and rhodium in bimetallic catalysts and possible reasons for the effects have been debated in the literature [1–3]. An important factor concerning the catalytic properties of bimetallic catalyst is the surface composition of the noble metal particles. There are several theoretical models, which have been used to predict the segregating component of bimetallic alloy [4–7]. However, these models are directly applicable only for clean samples of pure bimetallic alloys and cannot be used in the case of supported catalysts. Another important element concerning the catalytic properties is the interaction between the noble metal particles and the catalyst support. If this interaction is weak, high-temperature conditions may induce considerable particle-size growth of noble metal and therefore decrease in activity. γ-Alumina-supported platinum is proposed to form two different phases: at low Pt concentrations a two-dimensional dispersed phase on the surface of alumina and at higher concentrations a three-dimensional particulate phase exhibiting the physical properties of bulk platinum [8–10]. In the case of alumina-supported platinum catalysts the sintering of the dispersed particles is suggested to be an important factor in catalyst deactivation, indicating weak interaction between platinum and alumina [11]. The Pt $4d_{5/2}$ binding energies measured by XPS are reported to be about 314.2 eV for metallic platinum [10,12], 315.3 eV for dispersed platinum phase [10], and about 317 eV for PtO_2 [10]. Too strong metal–support interaction may also lead to decreased catalytic activity, as suggested for alumina-supported rhodium. At high-temperature aging

* Corresponding author. Fax +358 3 3115 2600.
E-mail address: mika.valden@tut.fi (M. Valden).

0021-9517/$ – see front matter
doi:10.1016/j.jcat.2004.05.033

in an oxidative atmosphere alumina-supported rhodium is known to form an oxide phase, which differs from "normal" Rh_2O_3. In aging, the amount of rhodium on the catalyst surface decreases and the detected rhodium oxide is characterized by its unusually high Rh $3d_{5/2}$ binding energy of about 310 eV and enhanced stability against H_2 reduction [13–15]. The mechanism of this strong interaction between rhodium and alumina is still unclear and has been explained by the diffusion of rhodium into the aluminum oxide [16–18], covering of the rhodium by a layer of alumina [19], or the formation of more stable oxide phase, RhO_2 on the surface of γ-Al_2O_3 [13]. The Rh $3d_{5/2}$ binding energy values for metallic rhodium are reported to be in the range of 307.0–307.3 eV [13] and for easily reducible Rh_2O_3 308.6–309.4 eV [13,20].

The atmosphere in a three-way catalyst is fluctuating continuously between reducing and oxidizing. For the conversion of NO, CO, and hydrocarbons, oxidation and reduction reactions must proceed simultaneously. Cerium oxide may be used as an oxygen-storage component to regulate the partial pressure of oxygen near the catalyst surface [21]. Oxidation and reduction reactions of ceria are fast and it is thus capable of storing oxygen during lean periods and releasing it during rich periods. The addition of zirconium to the cubic structure of ceria increases its thermal stability and improves its ability to store oxygen [22,23]. Ceria, zirconia, and Ce–Zr mixed oxides are widely used as an additive in alumina-supported catalysts and also as a catalyst support material. If rhodium is supported on pure Ce–Zr mixed oxide, the rhodium oxide phase formed in high-temperature air aging at 1000 °C has been demonstrated to be easily reducible [14].

In the present work Pt, Rh, and bimetallic Pt–Rh catalysts with pure alumina and Ce–ZrO_2-modified alumina washcoats were studied. The noble metals were impregnated either to calcined catalyst washcoat or to Ce–ZrO_2 powder, which was then used as a washcoat constituent. The main purpose of this study was to find out whether the synergistic effect of platinum and rhodium is capable of stabilizing alumina-supported rhodium against the formation of reduction-resistive oxide phase.

2. Experimental

The washcoats of Pt, Rh, and Pt–Rh catalysts composed either of pure γ-alumina or of La-stabilized (4 wt%) γ-alumina modified by $Ce_{0.18}Zr_{0.82}O_2$. The methods used in the noble metal addition were impregnation into the calcined washcoat or preimpregnation into the $Ce_{0.18}Zr_{0.82}O_2$ powder. The bimetallic catalysts were prepared using a conventional two-step aqueous incipient wetness impregnation procedure, where Rh was deposited first followed by Pt deposition using calculated concentrations to reach the desired precious metal content. Pt- and Rh-only catalysts were prepared in a similar manner. Washcoat slurry containing γ-alumina (90 wt%) and alumina sol (10 wt%) or in the case of Ce–ZrO_2 containing samples La-stabilized γ-alumina (50 wt%), Ce–ZrO_2 (40 wt%), and alumina sol (10 wt%) was first deposited onto a metal foil. The sample was then dried overnight at 110 °C in normal atmosphere and finally calcined in air for 4 h at 550 °C. Thereafter the precious metal was impregnated into the catalyst support and the sample was again dried overnight at 110 °C in normal atmosphere and calcined in air for 4 h at 550 °C. Alternatively, in the preimpregnation method, the precious metal was first impregnated into the Ce–ZrO_2 powder after which the precious metal containing Ce–ZrO_2 powder was used as a washcoat constituent together with La-stabilized γ-alumina and alumina sol. $[Pt(NH_3)_4] \cdot 2HCO_3$ and $Rh(NO_3)_3 \cdot 2H_2O$ were used as precious metal precursors in the impregnation. The precious metal loadings of Pt and Rh in the catalyst support were 0.5 and 0.2 wt%, respectively, except in the Pt/Al_2O_3 sample, where the Pt loading was 1 wt%. The addition method of platinum and rhodium was varied from sample to sample. For example the Pt/Ce–ZrO_2 + Rh + Al_2O_3 catalyst was prepared by first impregnating platinum into the Ce–ZrO_2 powder, which was then used as a washcoat component. Thereafter rhodium was impregnated into the catalyst supports and the catalyst was dried and calcined. Table 1 summarizes the compositions, the precious metal loadings, and the preparation methods of the samples investigated in this work. Catalyst aging was performed in a muffle furnace in ambient static air at normal atmospheric pressure for 3 h at 1000 °C. The reducibility of rhodium and platinum oxides formed in the aging was investigated by annealing the catalysts in situ in 400 mbar of static H_2 at 300 °C for 30 min followed by the XPS measurements.

The XPS experiments were carried out in a Kratos XSAM 800 electron spectrometer with a base pressure less than 1×10^{-8} mbar. Nonmonochromatic Mg$K\alpha$ X-rays were used as a primary excitation and the hemispherical energy analyser was operated in a fixed analyser transmission (FAT) mode with a pass energy of 38 eV. The Al 2p line at 74.2 eV was used as a binding energy reference together with the C 1s line at 284.6 eV. All binding energies quoted in this work were measured within a precision of ±0.2 eV. The inelastic background was removed from the spectra using Shirley's method for the noble metal spectra and linear background subtraction for the Ce 3d spectra.

The TEM measurements were carried out in a Jeol JEM 2010 AEM operated at 200 kV and equipped with a Noran Vantage energy-dispersive spectrometer. TEM samples were prepared by scraping the catalyst washcoat off from the metal foil and crushing it between glass slides. The powdered washcoat was dispersed onto a holey carbon-covered Cu grid with ethanol. The samples investigated after H_2 reduction were exposed to air between the reduction and the TEM analysis.

Table 1
The compositions, the noble metal loadings, and the manufacturing methods of the catalysts

Sample name	Washcoat composition	Noble metals (wt%)	Manufacturing method
Rh/Al_2O_3	γ-Al_2O_3	Rh 0.2	Rh impregn. to γ-Al_2O_3 washcoat
Pt/Al_2O_3	γ-Al_2O_3	Pt 1.0	Pt impregn. to γ-Al_2O_3 washcoat
$PtRh/Al_2O_3$	γ-Al_2O_3	Rh 0.2, Pt 0.5	Pt and Rh impregn. to γ-Al_2O_3 washcoat
$Rh + Al_2O_3 + Pt/Ce–ZrO_2$	La-stabilized γ-Al_2O_3, $Ce–ZrO_2$	Rh 0.2, Pt 0.5	Pt preimpregn. to $Ce–ZrO_2$, Rh impregn. to washcoat
$Pt + Al_2O_3 + Rh/Ce–ZrO_2$	La-stabilized γ-Al_2O_3, $Ce–ZrO_2$	Rh 0.2, Pt 0.5	Pt impregn. to washcoat, Rh preimpregn. to $Ce–ZrO_2$
$PtRh/Ce–ZrO_2 + Al_2O_3$	La-stabilized γ-Al_2O_3, $Ce–ZrO_2$	Rh 0.2, Pt 0.5	Pt and Rh preimpregn. to $Ce–ZrO_2$

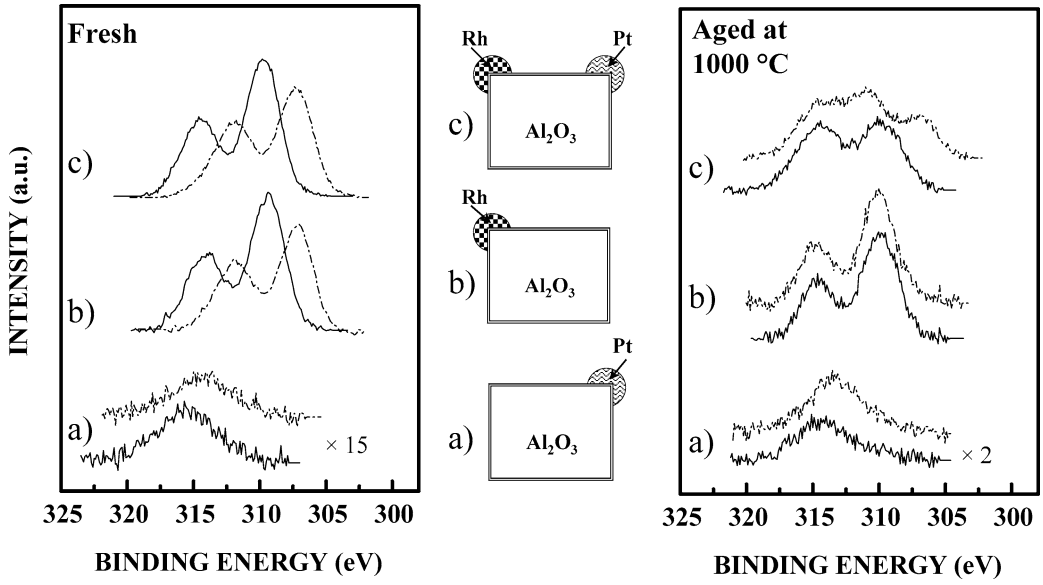

Fig. 1. Photoelectron spectra of the binding energy region containing Rh 3d and Pt $4d_{5/2}$ peaks for fresh (left) and 1000 °C air-aged (right) catalysts. (a) Pt/Al_2O_3; (b) Rh/Al_2O_3; (c) $PtRh/Al_2O_3$. The schematic pictures of the catalyst structures are shown. The spectrum with a solid line of each pair is measured from the as-received catalyst and the spectrum with a dotted line from the catalyst after in situ H_2 reduction.

3. Results

3.1. Rh 3d and Pt 4d XPS transitions

In Fig. 1 the XP spectra of the binding energy region containing Rh 3d and Pt $4d_{5/2}$ peaks are shown for fresh (left) and 1000 °C aged (right) catalysts. In these catalysts the noble metals are added to pure γ-alumina washcoat by impregnation and schematic pictures of the catalyst structures are also shown in the Fig. 1. The spectra (a) are measured from the Pt/Al_2O_3 catalyst, spectra (b) from the Rh/Al_2O_3 catalyst and spectra (c) from the $PtRh/Al_2O_3$ catalyst. The spectrum with a solid line of each pair is measured from the as-received catalyst and the spectrum with a dotted line from the catalyst after in situ H_2 reduction in 400 mbar at 300 °C for 30 min. On the fresh Rh/Al_2O_3 and $PtRh/Al_2O_3$ catalysts the Rh 3d transition is intensive and rhodium is reducible as indicated by the shift of the Rh $3d_{5/2}$ peaks from the binding energies of 309.4 and 309.6 eV, respectively, to 307.2 eV in the H_2 reduction. After air aging of the Rh/Al_2O_3 catalyst at 1000 °C, the intensity of the Rh 3d peaks has decreased and the Rh $3d_{5/2}$ binding energy has increased to 309.9 eV, which coincides with the peak position of reduction-resistive rhodium oxide phase. The H_2 reduction does not affect remarkably the peak position. In the aged $PtRh/Al_2O_3$ catalyst Rh 3d and Pt $4d_{5/2}$ peaks are overlapping, but the peak positions can be obtained by peak fitting. In the fitting procedure, the relative widths and areas as well as the distance between the Rh $3d_{5/2}$ and Rh $3d_{3/2}$ synthetic components were constrained virtually to the same values as for the fresh catalysts. An example of the result from similar fitting procedure is presented in our previous work [24]. In this catalyst rhodium appears to be in two different chemical states with the $3d_{5/2}$ binding energies of 310.2 and 308.4 eV. The higher value coincides with the peak position of reduction-resistive rhodium oxide and the lower is in the range of reducible Rh_2O_3. After the H_2 reduction of the aged catalyst the Rh $3d_{5/2}$ peak with higher binding energy remains at the same position, 310.2 eV. The lower binding energy component of the Rh $3d_{5/2}$ peak shifts to 306.8 eV, which is slightly lower than the binding energy range for metallic rhodium.

The chemical state of platinum was determined from the Pt $4d_{5/2}$ peak. This transition is wider and weaker than the most intensive Pt 4f transition and it also interferes with the Rh 3d peak pair. However, it is more clearly visible than the Pt 4f peak pair, which is interfering with the very intensive Al 2p peak. The variations of the small shoulder under the Al 2p peak caused by the Pt $4f_{7/2}$ peak were also

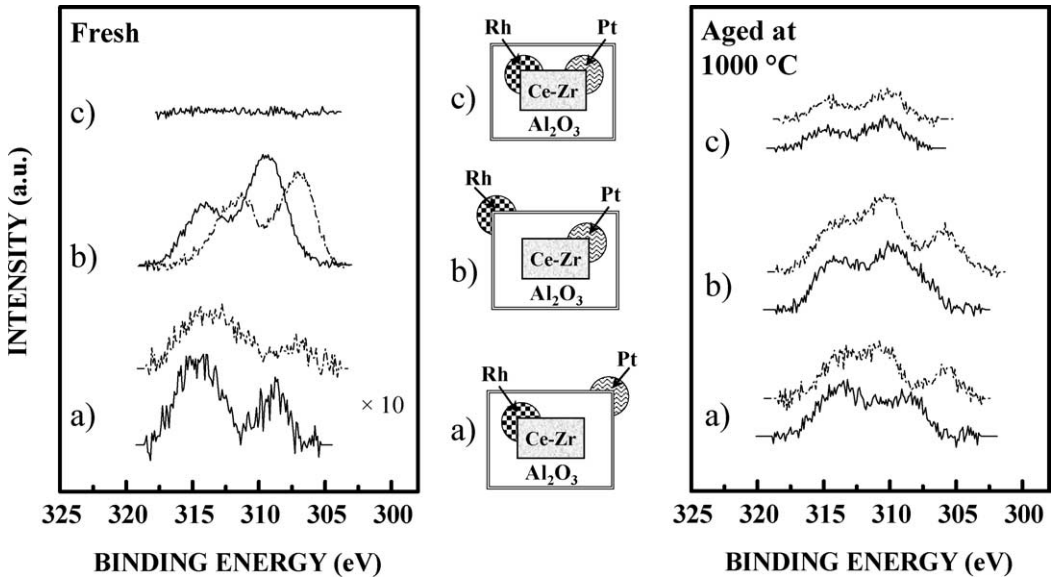

Fig. 2. Photoelectron spectra of the binding energy region containing Rh 3d and Pt $4d_{5/2}$ peaks for fresh (left) and 1000 °C air-aged (right) catalysts. (a) Pt + Al_2O_3 + Rh/Ce–ZrO_2 (Rh preimpregnated to Ce–ZrO_2, Pt impregnated to washcoat); (b) Rh + Al_2O_3 + Pt/Ce–ZrO_2 (Pt preimpregnated to Ce–ZrO_2, Rh impregnated to washcoat); (c) PtRh/Ce–ZrO_2 + Al_2O_3 (Pt and Rh preimpregnated to Ce–ZrO_2). The schematic pictures of the catalyst structures are shown. The spectrum with a solid line of each pair is measured from the as-received catalyst and the spectrum with a dotted line from the catalyst after in situ H_2 reduction.

followed and the peak shifts seemed to be about the same magnitude as those observed for the Pt $4d_{5/2}$ peak. On the fresh Pt/Al_2O_3 catalyst the Pt $4d_{5/2}$ peak is located at the binding energy of 315.5 eV and H_2 reduction shifts the peak to 314.4 eV, as seen in Fig. 1. Due to the high intensity of the Rh 3d peak pair the weak Pt $4d_{5/2}$ transition is not resolvable from the fresh PtRh/Al_2O_3 catalyst. After aging of the Pt/Al_2O_3 catalyst at 1000 °C the Pt $4d_{5/2}$ peak is at the binding energy of 314.1 eV and after the H_2 reduction of the aged catalyst the Pt $4d_{5/2}$ binding energy is 313.3 eV. After aging in air at 1000 °C the Pt $4d_{5/2}$ signal intensity from the bimetallic PtRh/Al_2O_3 catalyst is comparable to the Rh 3d transitions and the peak appears at the binding energy of 314.7 eV. In the H_2 reduction the peak is shifted to lower binding energy of 314.0 eV.

The XP spectra shown in Fig. 2 are measured from the catalysts where the noble metals were impregnated either to calcined catalyst washcoat or to Ce–ZrO_2 powder, which was then used as a washcoat constituent. The schematic pictures of the catalyst structures are again shown in the figure. Spectra (a) are measured from the Pt + Al_2O_3 + Rh/Ce–ZrO_2 catalyst, spectra (b) from the Rh + Al_2O_3 + Pt/Ce–ZrO_2 catalyst, and spectra (c) from the PtRh/Ce–ZrO_2 + Al_2O_3 catalyst. The spectrum with a solid line of each pair is measured from the as-received catalyst and the spectrum with a dotted line from the catalyst after H_2 reduction. On the fresh Rh + Al_2O_3 + Pt/Ce–ZrO_2 catalyst the Rh 3d transition is intensive and rhodium is reducible as indicated by the shift of the Rh $3d_{5/2}$ peak from the binding energy of 309.4 to 307.1 eV in the H_2 reduction. On the fresh PtRh/Ce–ZrO_2 + Al catalyst, where both Pt and Rh have been preimpregnated to Ce–ZrO_2 the noble metals are undetectable by XPS. On the fresh Pt + Al_2O_3 + Rh/Ce–ZrO_2 catalyst weak platinum Pt $4d_{5/2}$ and rhodium 3d signals can be detected and the binding energies are 308.9 eV for Rh $3d_{5/2}$ and 314.9 eV for Pt $4d_{5/2}$. In the H_2 reduction these binding energies shift to 307.2 and 314.1 eV, respectively. After air aging at 1000 °C rhodium is detectable by XPS from the PtRh/Ce–ZrO_2 + Al catalyst with the binding energy of 310.3 eV and the peak position is almost the same, 310.2 eV, also after the H_2 reduction. In the aged Rh + Al_2O_3 + Pt/Ce–ZrO_2 and Pt + Al_2O_3 + Rh/Ce–ZrO_2 catalysts both Rh $3d_{5/2}$ and Pt $4d_{5/2}$ peaks are visible and rhodium appears to be in two different chemical states. The Rh $3d_{5/2}$ binding energies for Rh + Al_2O_3 + Pt/Ce–ZrO_2 catalyst are 309.8 and 307.7 eV, and for Pt +Al_2O_3 + Rh/Ce–ZrO_2 catalyst 309.9 and 308.0 eV. The Pt $4d_{5/2}$ binding energies are 313.6 and 314.0 eV, respectively. After the H_2 reduction of the aged Rh + Al_2O_3 + Pt/Ce–ZrO_2 and Pt + Al_2O_3 + Rh/Ce–ZrO_2 catalysts the lower binding energy component of the Rh $3d_{5/2}$ peak shifts to 305.9 and 306.1 eV, respectively, and the other component remains at about the same binding energy. The fitted peak positions measured from the aged catalysts are listed in Table 2.

3.2. TEM characterization

Composition and microstructure of the catalysts were characterized by TEM. In all the fresh catalysts only small-grained γ-Al_2O_3 structures and, if present, Ce–ZrO_2 agglomerates are seen. The size of the Pt and Rh particles is too small to be resolvable from the washcoat by conventional TEM, as also observed in other studies [2]. According to the EDS analysis platinum and rhodium are rather evenly dis-

Table 2
The Rh $3d_{5/2}$ and Pt $4d_{5/2}$ XPS binding energy values measured from the air-aged catalysts as received and after in situ H_2 reduction and average noble metal particle sizes measured from the catalysts by TEM

Sample name	Rh $3d_{5/2}$ (A)		Rh $3d_{5/2}$ (B)		Pt $4d_{5/2}$		Av. particle size	
	As rec.	H_2 red.	As rec.	H_2 red.	As rec.	H_2 red.	As rec.	H_2 red.
Rh/Al_2O_3			309.9 eV	310.0 eV			< 20 nm	< 20 nm
Pt/Al_2O_3					314.1 eV	313.3 eV	120 nm	120 nm
$PtRh/Al_2O_3$	308.4 eV	306.8 eV	310.2 eV	310.2 eV	314.7 eV	314.0 eV	130 nm	130 nm
$Rh + Al_2O_3 + Pt/Ce–ZrO_2$	307.7 eV	305.9 eV	309.8 eV	310.0 eV	313.6 eV	313.1 eV	230 nm	360 nm
$Pt + Al_2O_3 + Rh/Ce–ZrO_2$	308.0 eV	306.1 eV	309.9 eV	309.9 eV	314.0 eV	313.4 eV	170 nm	360 nm
$PtRh/Ce–ZrO_2 + Al_2O_3$			310.3 eV	310.2 eV			180 nm	260 nm

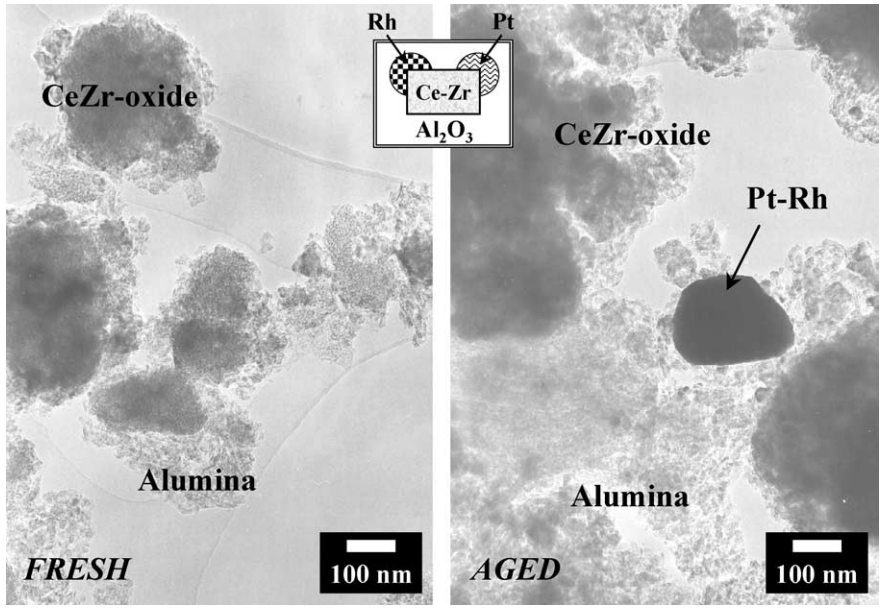

Fig. 3. The microstructure of the $Rh/Ce–ZrO_2 + Al_2O_3$ catalyst (Pt and Rh preimpregnated to $Ce–ZrO_2$) as fresh and after air aging.

tributed to the washcoat. In the aged catalysts, the grain size of the γ-Al_2O_3 and $Ce–ZrO_2$ has slightly increased and in the case of the Pt-only and Pt–Rh bimetallic catalysts the noble metal particles can also be resolved from the washcoat. In the aged Rh-only catalyst the noble metal particle size stays below 20 nm, which is approximately the grain size of γ-Al_2O_3 after aging and the Rh particles cannot be resolved from the washcoat by conventional TEM. The structure of the $PtRh/Ce–ZrO_2 + Al_2O_3$ catalyst as fresh and after air aging is shown in Fig. 3 and the structure was similar in the case of the other catalysts. The results of the EDS analysis indicate that in all the aged bimetallic catalysts the noble metal particles contain both platinum and rhodium and the core of each particle is Pt rich and the surface Rh rich. Weak signals of both noble metals are also obtained by EDS from those parts of the washcoat, where no noble metal particles are seen. In several previously reported studies the segregating component of bimetallic alloy has been shown to depend on the surrounding atmosphere. During the heat treatment in an oxidative atmosphere rhodium segregates onto the surface of Pt–Rh alloy and in a reductive atmosphere the segregating component is platinum [1,25,26]. On the basis of the previous studies the segregation of rhodium on the particle surface in the high-temperature air aging of the catalysts is an expected result. The particle-size distributions are shown in Figs. 4 and 5 for the catalysts, where the particle size was detectable after the aging treatment. The particle detection limit determined by γ-alumina grain size, 20 nm, is marked as a low limit in the diagrams. To obtain these distributions the diameters of 150 particles per sample were measured after aging in air at 1000 °C and also after H_2 reduction of the aged catalyst. As can be seen from Fig. 4 the distributions for the Pt/Al_2O_3 and $PtRh/Al_2O_3$ catalysts with pure γ-alumina washcoat are almost similar. H_2 reduction does not affect the average particle size. However, the particle-size distributions shown in Fig. 5 for the catalysts with γ-alumina washcoat modified by $Ce–ZrO_2$ and La_2O_3 differ remarkably from the distributions for pure γ-alumina-supported catalysts. In these catalysts the particle-size growth in aging has been more pronounced and the H_2 reduction has increased the average size of the particles even further. The average noble metal particle sizes measured from the catalysts are listed in Table 2 together with the binding energy values from the aged catalysts.

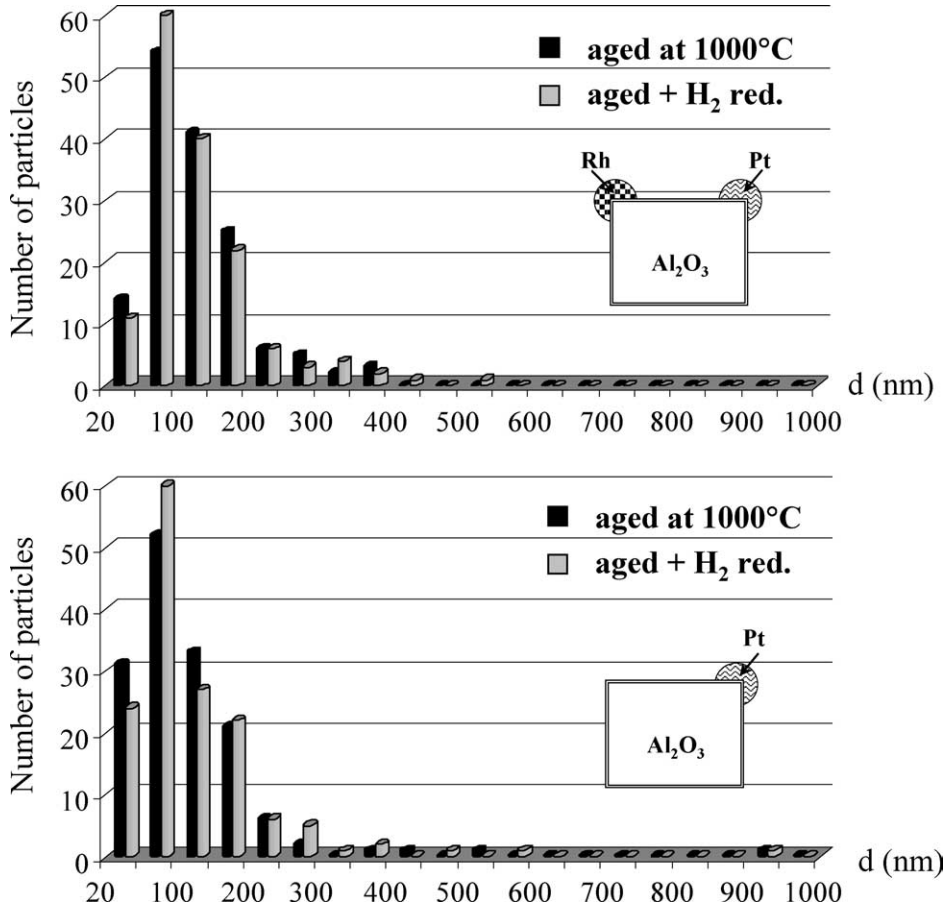

Fig. 4. The particle-size distributions for the air-aged Pt/Al_2O_3 and $PtRh/Al_2O_3$ catalysts. The schematic pictures of the catalyst structures are shown.

3.3. Ce 3d XPS transition

$Ce–ZrO_2$ and lanthanum oxide were used as additives in the preparation of the catalysts and the changes of the oxidation states of Zr, La, and Ce induced by air-aging treatment or in situ H_2 reduction were also followed by XPS. According to Zr 3d and La 3d spectra the oxidation states of zirconium and lanthanum remain practically unchanged both in the air-aging treatment and in the H_2 reduction. The Zr $3d_{5/2}$ peak is located at the binding energy of about 182.0 eV, which coincides with the values measured from Ce–Zr mixed oxides [27]. The La $3d_{5/2}$ peak is at the binding energy of about 835.5 eV, which falls in the range measured for the dispersed lanthanum phase [28]. The Ce 3d spectra from cerium-containing oxides is known to be complicated because of the hybridization of the O 2p valence band with the Ce 4f orbital [29,30]. If both Ce^{3+} and Ce^{4+} oxidation states are present in the sample, five spin–orbit duplets can be found in the Ce 3d region. In addition, the experimental procedure of XPS measurements may cause partial reduction of cerium oxide. The exposure to the X-ray beam, vacuum environment, secondary electrons from the X-ray source, or sample charging may contribute to the damage of the sample [31]. However, all the catalysts studied in this work have been exposed to similar measurement conditions; thus, the Ce 3d spectra can be compared. In Fig. 6 the Ce 3d spectra from the $Pt/Ce–ZrO_2 + Rh + Al_2O_3$ catalyst is shown after aging in air and after H_2 reduction of the aged catalyst. The peak positions of the duplets caused by Ce^{3+} and Ce^{4+} oxidation states are marked into the figure according to the notation first used by Burroughs et al. [32]. The peak pairs $v_0–u_0$ and $v'–u'$ are characteristic for the Ce^{3+} oxidation state and the other peak pairs are due to Ce^{4+} state. In the transition from Ce^{4+} to more reduced Ce^{3+} form, the most obvious features appearing in the spectra are a decrease in the intensity of u''' and v'' peaks at the binding energies of about 917 and 889.5 eV and an increase in v' at about 885 eV. From the Ce 3d spectra it can be deduced that in the air-aged $Pt/Ce–ZrO_2 + Rh + Al_2O_3$ catalyst cerium is mostly at Ce^{4+} oxidation state, but also some Ce^{3+} state seems to be present. After the in situ H_2 reduction the u''' peak due to the Ce^{4+} state is absent indicating pure Ce^{3+} state. The Ce 3d spectra from all the $Ce–ZrO_2$-containing catalysts, both fresh and aged, were very much similar as seen in Fig. 7 showing the Ce 3d spectra from fresh and aged $Pt + Al_2O_3 + Rh/Ce–ZrO_2$, $Rh + Al_2O_3 + Pt/Ce–ZrO_2$, and $PtRh/Ce–ZrO_2 + Al_2O_3$ catalysts. For the fresh catalysts the signal intensity is lower, but the shape of the spectra is the same. According to these results, cerium is in reducible form in all the $Ce–ZrO_2$-containing catalysts and

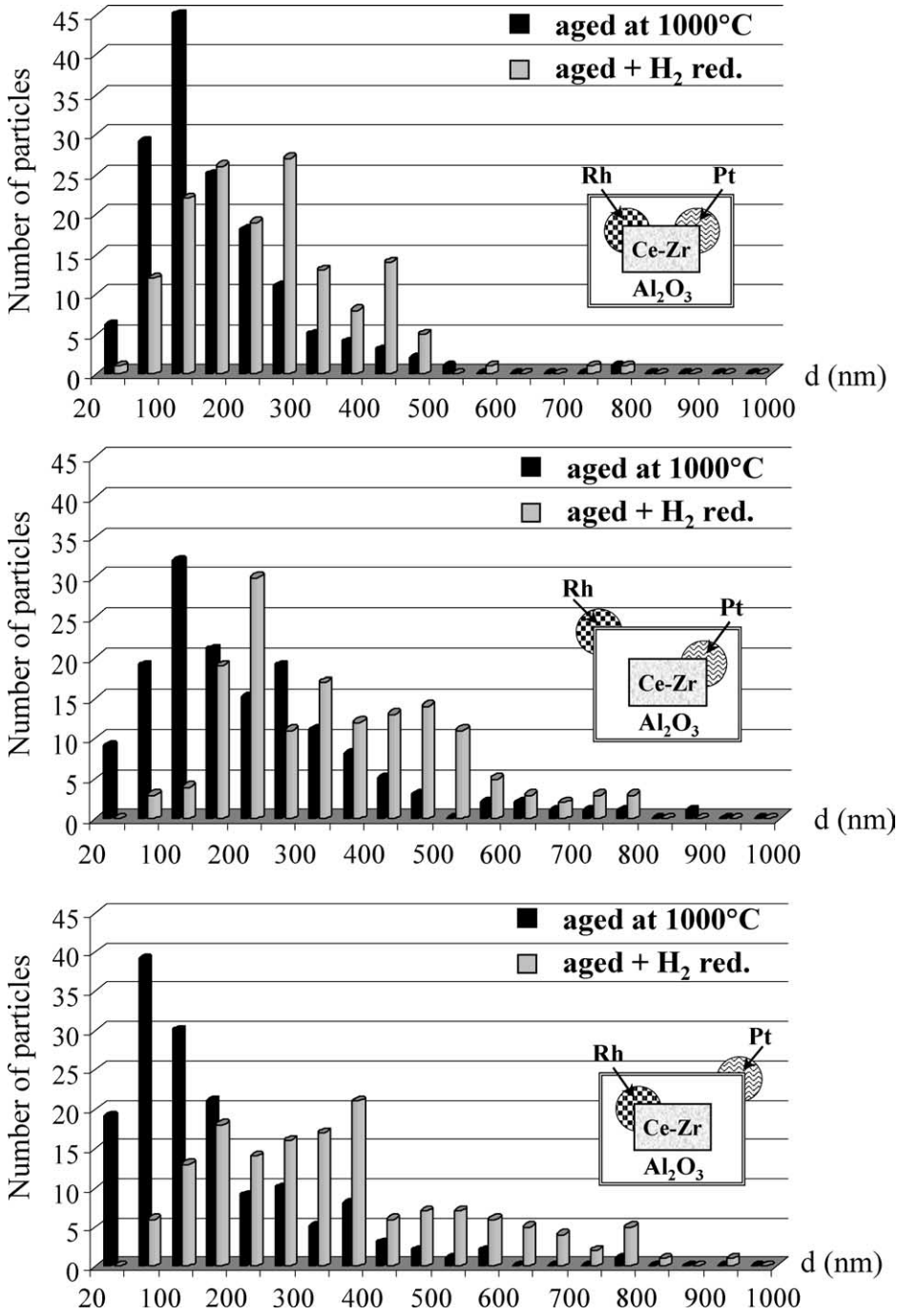

Fig. 5. The particle-size distributions for the air-aged Pt + Al_2O_3 + Rh/Ce–ZrO_2 (Rh preimpregnated to Ce–ZrO_2, Pt impregnated to washcoat), Rh + Al_2O_3 + Pt/Ce–ZrO_2 (Pt preimpregnated to Ce–ZrO_2, Rh impregnated to washcoat), and PtRh/Ce–ZrO_2 + Al_2O_3 (Pt and Rh preimpregnated to Ce–ZrO_2) catalysts. The schematic pictures of the catalyst structures are shown.

seems to be capable of acting as an oxygen-storage component releasing oxygen in a reducing atmosphere.

4. Discussion

Metal particle sintering is a thermally activated process, which may occur by three different mechanisms: (i) particle migration and coalescence on the support surface, (ii) atom emission from smaller particles and recapture to larger ones (Ostwald ripening), and (iii) vapor-phase transport. All these mechanisms play a role in the noble metal particle-size growth on supported catalysts. In air aging at 1000 °C the particle-size growth of platinum is more prominent than that of the rhodium, due to the following reasons: the higher loading of platinum in the catalyst, the lower stability of platinum oxide and the strong interaction of rhodium with the

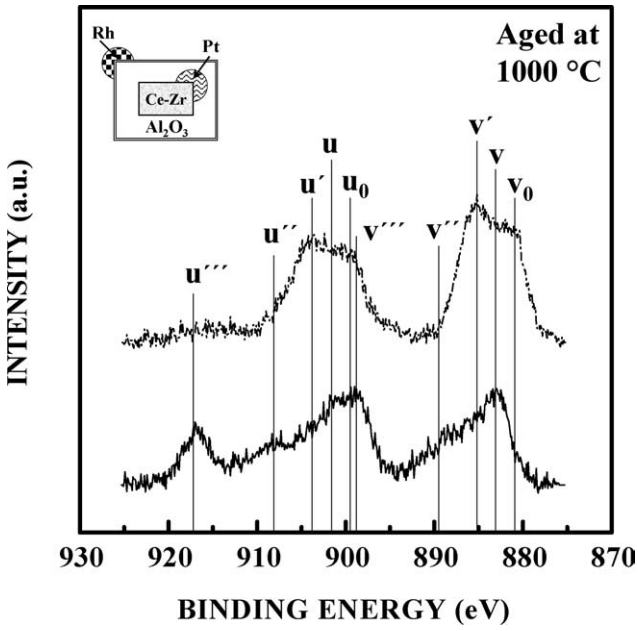

Fig. 6. Ce 3d photoelectron spectra from the Rh + Al_2O_3 + Pt/Ce–ZrO_2 catalyst after aging in air (solid line) and after H_2 reduction of the air-aged catalyst (dotted line). The peak positions of the douplets caused by Ce^{3+} and Ce^{4+} oxidation states are marked into the figure according to the notation by Burroughs et al. [32].

alumina support. The majority component of the bimetallic particles formed is therefore platinum. The relatively stable rhodium oxide segregating on the surface of the bimetallic particles is expected to retard the particle-size growth in comparison to the platinum-only catalyst. However, this is not seen in the samples of this work, since the particle-size distributions of the alumina-supported platinum-only and Pt–Rh samples are similar after air aging.The vapor-phase transport of both platinum and rhodium on γ-alumina support has been reported to be greatly enhanced by the presence of CeO_2 at temperatures between 800 and 900 °C in air atmosphere [33]. The volatile noble metal oxides are suggested to be responsible for the vapor-phase transport in oxidizing atmosphere. The more pronounced noble metal particle-size growth in 1000 °C air aging detected on the Ce–ZrO_2-containing catalysts studied in this work might reflect this phenomenon. The noble metal particle size was also found to increase in the low-temperature hydrogen reduction on the Ce–ZrO_2-containing catalysts. The explanation for this may be related to the ability of Ce–ZrO_2 to store and release oxygen. As seen from the Ce 3d spectra in Fig. 6, cerium oxide is reduced in the hydrogen treatment and the released oxygen may combine with hydrogen on the surface of the noble metals. The water vapor thus formed may induce remarkable local increase of humidity in the pores of the catalyst support and turn the hydrogen reduction to low-temperature hydrothermal aging. This may, in turn, lead to more pronounced particle-size growth, since the presence of water vapor in the aging atmosphere is known to favor the particle sintering of bimetallics similar to that observed for monometallics [34].

On the fresh catalysts, both platinum and rhodium are highly dispersed regardless of the manufacturing method. Rhodium is present in the form of easily reducible rhodium oxide. On PtRh/Ce–ZrO_2 + Al_2O_3 and Pt + Al_2O_3 + Rh/Ce–ZrO_2 catalysts, where rhodium has been added by preimpregnation to the Ce–ZrO_2, the visibility of Rh 3d peaks is poor and in the case of PtRh/Ce–ZrO_2 + Al_2O_3 catalyst Rh 3d cannot be detected by XPS. This is probably related to the manufacturing process, where Rh is first incorporated to the Ce–ZrO_2 powder and the Rh/Ce–ZrO_2 precursor material is then added to the alumina slurry. In this process the rhodium-containing Ce–ZrO_2 agglomerates are partially encapsulated by a porous layer of alumina [14]. The Rh $3d_{5/2}$ binding energies of the easily reducible rhodium oxide on the fresh catalysts are found to be in the range of 308.9–309.6 eV. After H_2 reduction the Rh $3d_{5/2}$ binding energies are between 307.1 and 307.2 eV that are characteristic for metallic rhodium. Platinum $4d_{5/2}$ peaks can be detected by XPS from the fresh Pt/Al_2O_3 and Pt + Al_2O_3 + Rh/Ce–ZrO_2 catalysts. The FWHM value for the $4d_{5/2}$ peak from the fresh catalysts is about 6 eV, suggesting the presence of several oxidation states. Since no clear shoulders are visible for fitting it can only be deduced that platinum is at least mostly in the oxidized form and is reducible by H_2 reduction as indicated by the shift in the average binding energy value of Pt $4d_{5/2}$ peak for about 1 eV.

In the aged Rh/Al_2O_3 catalyst the particle size of rhodium stays below 20 nm, which is approximately the grain size of γ-Al_2O_3 after aging and the Rh particles cannot be detected by conventional TEM. Rhodium is present as a reduction-resistive oxide phase with high Rh $3d_{5/2}$ binding energy of about 310 eV. The binding energy of this peak is not affected by H_2 reduction at 300 °C. However, besides the high binding energy component also another Rh 3d peak pair appears at lower binding energy (307.7–308.4 eV) on the PtRh/Al_2O_3, Pt + Al_2O_3 + Rh/Ce–ZrO_2, Rh + Al_2O_3 + Pt/Ce–ZrO_2, and PtRh/Ce–ZrO_2 + Al_2O_3 catalysts. This form of rhodium oxide is reducible as indicated by the shift of the peak to lower binding energies in the H_2 reduction. During aging in air, bimetallic Pt–Rh particles are formed and rhodium is found to segregate onto the surface of these particles. Both platinum and rhodium are also detected to be present in those parts of the support, where noble metal particles are not visible. In the previous studies the magnitude of the binding energy shifts due to alloying has been detected to be so small that the peaks from pure Pt or Rh are impossible to resolve by fitting from the peaks originating from the alloy particles on catalyst support. This is partly due to the large linewidth of the peaks originating from supported particles [1,20]. The two different states of rhodium in bimetallic catalysts after air aging are suggested to be rhodium oxide in strong interaction with alumina support (high binding energy of about 310 eV, reduction-resistive) and rhodium oxide on the surface of Pt–Rh bimetallic particles (lower bind-

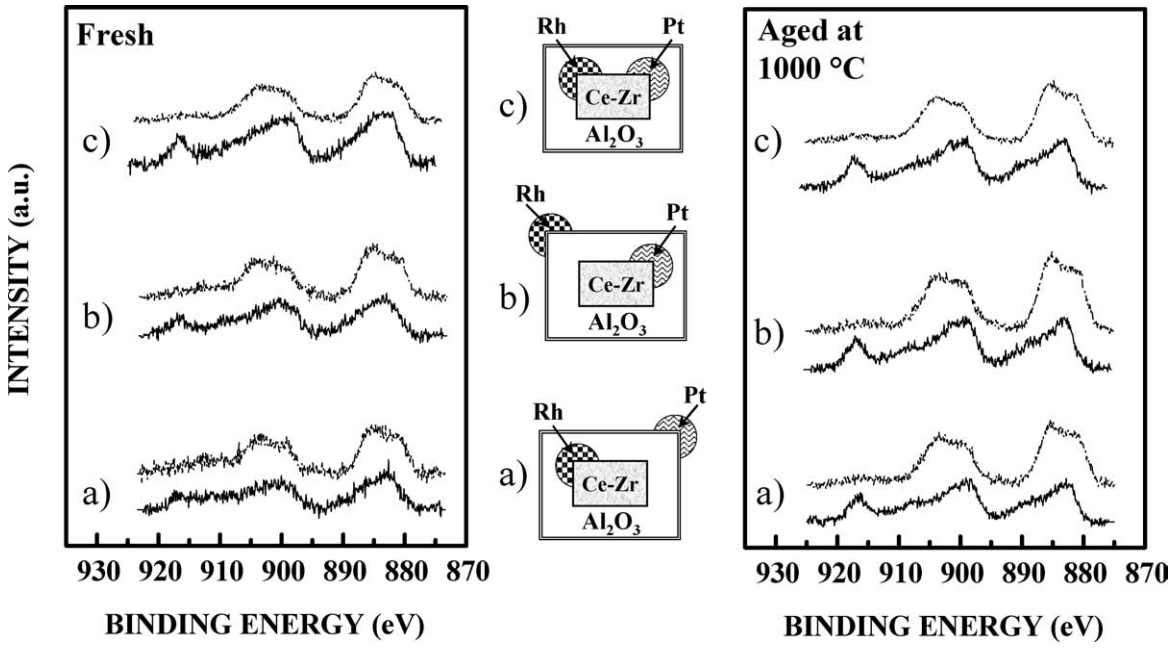

Fig. 7. Ce 3d photoelectron spectra of fresh (left) and 1000 °C aged catalysts (right) measured as received (solid line) and after H_2 reduction (dotted line). The schematic pictures of the catalyst structures are shown. (a) Pt + Al_2O_3 + Rh/Ce–ZrO_2 (Rh preimpregnated to Ce–ZrO_2, Pt impregnated to washcoat); (b) Rh + Al_2O_3 + Pt/Ce–ZrO_2 (Pt preimpregnated to Ce–ZrO_2, Rh impregnated to washcoat); (c) PtRh/Ce–ZrO_2 + Al_2O_3 (Pt and Rh preimpregnated to Ce–ZrO_2).

ing energy, reducible). In the bimetallic PtRh catalyst the Rh–alumina interaction has been partly substituted by the stronger interaction between platinum and rhodium and thus part of the rhodium oxide has remained in reducible form in air aging. The absence of the reducible low binding energy component on the Rh 3d spectra of the PtRh/Ce–ZrO_2 + Al_2O_3 catalyst is probably due to the encapsulation of noble metal containing Ce–ZrO_2 agglomerates by a porous layer of alumina. The detected rhodium signal mostly originates from the aluminum oxide layer, where rhodium is in the reduction resistive form.

After H_2 reduction the binding energy of the reducible Rh 3d pair is lower than the values usually reported for metallic rhodium on a catalyst surface (307.0–307.3 eV) [13,14]. An explanation for the unusually low Rh 3d binding energy might be differential charging. In air-aging bimetallic Pt–Rh particles are formed and the particle-size growth is remarkable. During XPS measurements the large metallic particles are differentially charged compared to the ceramic support structure or the finely dispersed particles [35,36]. Differential charging seems to be more pronounced in the case of the Ce–ZrO_2-containing catalysts, where the average particle size after H_2 reduction is larger than in the PtRh/Al_2O_3 catalyst. In these catalysts platinum also shows binding energy values lower than usually reported for metallic platinum.

5. Conclusions

The synergistic effect of platinum and rhodium is shown to be capable of stabilizing rhodium against the formation of a reduction-resistive oxide phase on alumina support. In the air aging at 1000 °C for 3 h, bimetallic PtRh particles are formed and the core of the particles is found to be Pt rich and the surface Rh rich. Rhodium is found to exist in two different states in bimetallic catalysts. The two Rh 3d peak pairs seen in the XP spectra are suggested to originate from rhodium oxide in strong interaction with alumina support (high binding energy of about 310 eV, reduction-resistive) and rhodium oxide on the surface of Pt–Rh bimetallic particles (lower binding energy, reducible). In the bimetallic PtRh catalyst the Rh–alumina interaction has been partly substituted by the stronger interaction between platinum and rhodium and thus part of the rhodium oxide has remained in reducible form in air aging.

The noble metal particle-size growth in aging treatment has been more pronounced on the Ce–ZrO_2-containing catalysts compared to the ones with pure alumina support and further increase of the particle size is detected on the Ce–ZrO_2-containing catalysts after H_2 reduction at 300 °C. This may be related to the ability of Ce–ZrO_2 to release oxygen in a reducing atmosphere. The released oxygen may combine with hydrogen on the surface of noble metals and the water vapor formed may induce remarkable local increase of humidity in the pores of the catalyst support, thus favoring the particle sintering.

Acknowledgment

The authors acknowledge M.Sc. Mari Honkanen and M.Sc. Tomi Kanerva for their contribution to the TEM ex-

periments and the Academy of Finland and the Finnish Cultural Foundation for financial support.

References

[1] R.E. Lakis, C.E. Lyman, H.S. Stenger, J. Catal. 154 (1995) 261.
[2] Z. Hu F.M. Allen, C.Z. Wan, R.M. Heck, J.J. Steger, R.E. Lakis, C.E. Lyman, J. Catal. 174 (1998) 13.
[3] A.G. van den Bosh-Driebergen, M.N.H. Kieboom, A. van Dreumel, R.M. Wolf, F.C.M.J.M. van Delft, B.E. Nieuwenhuys, Catal. Lett. 2 (1989) 73.
[4] R.A. Van Santen, W.M.H. Sachtler, Appl. Surf. Sci. 3 (1979) 121.
[5] D. Winblatt, R.C. Ku, Appl. Surf. Sci. 65 (1987) 511.
[6] A.D. Van Langeveld, J.W. Niemantsverdriet, Surf. Sci. 178 (1986) 880.
[7] B. Legrand, G. Treglia, Surf. Sci. 236 (1990) 398.
[8] H.C. Yao, M. Sieg, H.K. Plummer, J. Catal. 59 (1979) 365.
[9] K. Otto, H.C. Yao, J. Catal. 66 (1980) 229.
[10] J.Z. Shyu, K. Otto, Appl. Surf. Sci 32 (1988) 246.
[11] Y.F. Chu, E. Ruckenstein, J. Catal. 55 (1978) 281.
[12] T.H. Ruhle, H. Schneider, J. Find, D. Herein, N. Pfänder, U. Wild, R. Schlögl, D. Nachtigall, S. Artelt, U. Heinrich, Appl. Catal. B 14 (1997) 69.
[13] Z. Weng-Sieh, R. Gronsky, A.T. Bell, J. Catal. 170 (1997) 62.
[14] S. Suhonen, M. Valden, M. Hietikko, R. Laitinen, A. Savimäki, M. Härkönen, Appl. Catal. A 218 (2001) 151.
[15] S. Suhonen, M. Hietikko, R. Polvinen, M. Valden, R. Laitinen, K. Kallinen, M. Härkönen, Surf. Interface Anal. 34 (2002) 76.
[16] H.C. Yao, S. Japar, M. Shelef, J. Catal. 50 (1977) 407.
[17] M. Shelef, G.W. Graham, Catal. Rev.-Sci. Eng. 36 (1994) 433.
[18] C. Wong, R. McCabe, J. Catal. 119 (1989) 47.
[19] J.G. Chen, M.L. Colaianni, P.J. Chen, J.T. Yates, G.B. Fisher, J. Phys. Chem. 94 (1990) 5059.
[20] J.L.G. Fierro, J.M. Palacios, F. Tomas, Surf. Interface Anal. 13 (1988) 25.
[21] K.C. Taylor, Catal. Rev.-Sci. Eng. 35 (1993) 457.
[22] J.R. González-Velasco, M.A. Gutiérrez-Ortiz, J-L. Marc, J.A. Botas, M.P. González-Marcos, G. Blanchard, Appl. Catal. B 25 (2000) 19.
[23] P. Fornasiero, G. Balducci, R. Di Monte, J. Kaspar, V. Sergo, G. Gubitosa, A. Ferrero, M. Graziani, J. Catal. 164 (1996) 173.
[24] R. Polvinen, M. Vippola, M. Valden, T. Lepistö, A. Suopanki, M. Härkönen, Surf. Interface Anal., in press.
[25] B.M. Joshi, H.S. Gandhi, M. Shelef, Surf. Coating Technol. 29 (1986) 131.
[26] Y. Matsumoto, Y. Okawa, T. Fujita, K.-I. Tanaka, Surf. Sci. 335 (1996) 109.
[27] A.E. Nelson, K.H. Schulz, Appl. Surf. Sci. 210 (2003) 206.
[28] L.P. Haack, J.E. deVries, K. Otto, M.S. Chattha, Appl. Catal. A 82 (1992) 199.
[29] A. Kotani, T. Jo, J.C. Parlebas, Adv. Phys. 37 (1988) 37.
[30] E. Wuilloud, B. Delley, W.D. Schneider, Y. Baer, Phys. Rev. Lett. 53 (1984) 202.
[31] J. E1 Fallah, L. Hilaire, M. Roméo, F. Le Normand, J. Electron Spectrosc. Relat. Phenom. 73 (1995) 89.
[32] P. Burroughs, A. Hamnett, A.F. Orchard, G. Thornton, J. Chem. Soc., Dalton Trans. 17 (1976) 1686.
[33] Y.-F. Yu-Yao, J.T. Kummer, J. Catal. 106 (1987) 307.
[34] J. Barbier, D. Duprez, Appl. Catal. B 4 (1994) 105.
[35] T.L. Barr, J. Vac. Sci. Technol. A 7 (1989) 1677.
[36] L. Guczi, R. Sundararajan, Z. Koppány, Z. Zsoldos, Z. Schay, F. Mizukami, S. Niwa, J. Catal. 167 (1997) 482.